The Structural Mechanics of Rail Guns With Discrete Supports Showing the Influence of DES

Liudas Tumonis, Markus Schneider, Rimantas Kačianauskas, and Vaidas Vadluga

***Abstract*—The dynamic behavior of the rail-gun housing, which includes the rails, is of great importance for the performance of the rail-gun system as a whole. As in the case of conventional guns, the mechanical response of the housing under transient loading (magnetic pressure) can lead to disturbances of the projectile trajectory due to momentum transfer. However, in the case of rail guns, these disturbances can be even more severe as the armature performance can be very sensitive to variations of the normal forces at the contact interface. In previous developments, the structural mechanics of a rail gun with discrete supports were analyzed using the conventional boundary conditions. In this paper, further considerations are focused on describing a specific distributed energy storage (DES) operation technique which was developed at ISL. Using the finite-element technique, numerical calculations were performed for the ISL rail-gun EMA3 equipped with a one-stage DES. Its caliber was 15 mm × 30 mm and produced a typical muzzle velocity of up to 1600 m/s, as well as peak currents of about 600 kA. Three spatially different DES configurations were used. The obtained results were then compared to the conventional breech-fed configuration.**

***Index Terms*—Dynamics, electromagnetic rail gun, finite-element method (FEM), rail-gun power supplies.**

I. Introduction

THE DYNAMIC interaction between the armatures and the rails at their contact interfaces is of prime importance for rail-gun technology. The mechanical response of the housing to the transient loading (magnetic pressure) can lead to considerable deformations of the rails, particularly at the positions where the projectile is located [1]–[5]. The contact performance of the armature is usually very sensitive to variations of the normal forces at the armature/rail interface [6]. Therefore, the evaluation of the displacement of the rail surfaces due to the effects of elastic surface waves is a mandatory calculation when designing such systems.

The structural analysis of the rail-gun system can be decoupled from the electromagnetic phenomena occurring at the first stage [2]–[5]. Moreover, the dynamics of the rail-gun housing can be treated as being independent of the behavior of the projectile itself. The magnetic pressure, which repels the rails from each other and which increases as the projectile speeds up, serves as a force boundary condition for purely mechanical calculations. While such investigations have been conducted for continuous support [2]–[4] and discrete support [1], [5] rail guns, this paper focuses on a specific type of rail gun, characterized as using the so-called distributed energy storage (DES) mode [7].

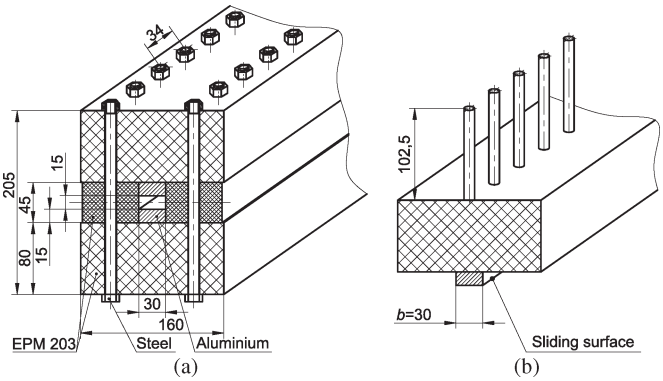

Fig. 1. Rail-gun structure. (a) Cross section. (b) Simplified model.

DES operation means that the current is injected not only at the breech end of the rails but also along the length of the launcher. One of the advantages gained from this mode is that the ohmic losses in the rails are reduced. Thus, when compared to a breech-fed rail gun, its efficiency is increased. The effects of DES on rail guns having discrete supports have been studied at ISL for more than ten years [8], [9]. The question of how DES influences the gun's structural mechanics was first addressed for a spatially fixed DES configuration [10]. In this paper, this issue is more fully analyzed with respect to the spatial and temporal configurations of the DES current injections.

II. Rail Geometry and Material Data

The ISL rail gun investigated was the EMA3 having a length of 3 m and a caliber of 15 mm × 30 mm. A view of the rail gun's cross section is presented in Fig. 1(a). Here, all sizes are given in millimeters.

In order to withstand the high forces repelling the rails from each other, the housing is constructed from a combination of bars made of an EPM 203 glass fiber reinforced plastic material (section size is 160 mm × 80 mm) and symmetrically located steel bolts. This housing design allows not only relatively quick mounting/dismounting but also taking of flash radiographs during the acceleration phase [11]. The rails (section size $b =$ 30 mm × 15 mm) were made of aluminum. Multiple brush armatures were used during the experiments.

Considering the axial symmetry of the rail, only half of its composite cross section was investigated. A simplified model of

Manuscript received February 11, 2010; revised July 26, 2010; accepted August 17, 2010. Date of publication October 11, 2010; date of current version January 7, 2011.

L. Tumonis, R. Kačianauskas, and V. Vadluga are with the Vilnius Gediminas Technical University, 10223 Vilnius, Lithuania.

M. Schneider is with the French–German Research Institute of Saint Louis, 68301 Saint-Louis, France.

Color versions of one or more of the figures in this paper are available online at http://ieeexplore.ieee.org.

Digital Object Identifier 10.1109/TPS.2010.2072519

TABLE I
MATERIAL PROPERTIES

Structural members	Materials	Physical properties
Rail	Aluminum	Density: $\rho = 2.75$ g/cm^3 Elast. modulus: $E = 69$ GPa Poisson's ratio: $\nu = 0.3$
Bolt	Steel	Density: $\rho = 8.9$ g/cm^3 Elast. modulus: $E = 207$ GPa Poisson's ratio: $\nu = 0.3$
Housing	EPM 203	Density: $\rho = 1.85$ g/cm^3 Elast. modulus: $E = 18$ GPa Poisson's ratio: $\nu = 0.3$

the rail-gun structure is presented in Fig. 1(b). Here, two section bolts were modeled as a single rod located in the section's center.

The properties of the materials used in the numerical tests of the rail gun are given in Table I.

III. RAIL LOADING

Instead of considering the distribution of the current between the different brushes leading to a corresponding spatial extension of the pressure gradient, the profile of the magnetic pressure load $q(x,t)$ is presented in a form of a step function

$$q(x,t) = p(t)H\left(x_f(t) - x\right). \tag{1}$$

Here, $H(x)$ is the heavy-side function. Since magnetic diffusion is neglected, the magnetic pressure $p(t)$ at time instant t is uniformly distributed along the rail between zero and the front position of the projectile denoted by x_f. The pressure jump point $x_f(t)$ corresponds precisely to the location of the current-carrying armature of the projectile.

This can be obtained by integrating the projectile velocity v

$$x_f(t) = \int_0^t v(\tau)d\tau. \tag{2}$$

The experimentally measured time variation of the velocity $v(t)$ of the projectile and the calculated time variation of its front position $x_f(t)$ obtained according to (2) are given in Fig. 2. The front position $x_f(t)$ is elaborated to define the loaded area.

The transient loading of the gun rail is of two types: conventional or the so-called breech-fed loading and DES loading. Breech-fed loading $p_{\mathrm{BR}}(x,t)$ is applied to the feed point A located at the breech of the rail gun. According to (1), this is characterized by the spatially constant pressure profile $p_{\mathrm{BR}}(x,t) = p_{\mathrm{BR}}(t)$.

The EMA3 rail gun can be equipped with a maximum of three DES stages. The experimental current profiles used in this experiment were obtained in a one-stage DES configuration.

The nature of the DES pressure load is, however, more complex and is characterized by the combined transient pressure profiles, which are generated at the two different current injection points A and B. A is the starting point discussed earlier, and B is the second point defined by the variable coordinate x_B. As

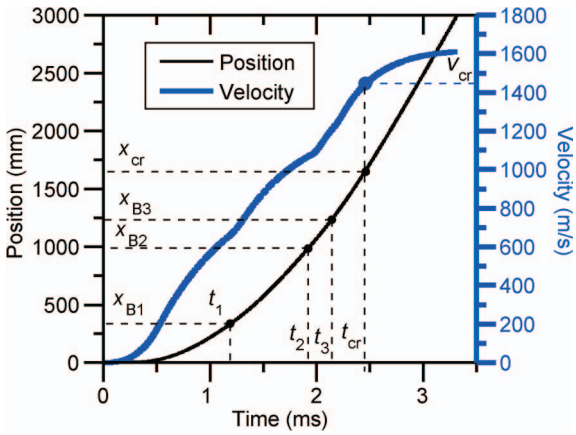

Fig. 2. Profiles of the velocity and front position of a projectile accelerated using the EMA3 rail gun.

a result, the loading area of the rail is divided into two parts. In the first part, when $x < x_B$, the pressure is denoted by $p_A(t)$ while, in the second part, when $x \geq x_B$, the pressure is denoted by $p_B(t)$.

On a formal basis, the DES-type pressure distribution $p_{\mathrm{DES}}(x)$ on the rail presents a discontinuous step function composed of the two time histories $p_A(t)$ and $p_B(t)$.

Consequently, the pressure distribution is time history dependent. It is defined as

$$p_{\mathrm{DES}}(x,t) = \begin{cases} p_A(t), & \text{if } x < x_B \\ p_B(t), & \text{if } x \geq x_B. \end{cases} \tag{3}$$

When $p(x) = p_{\mathrm{DES}}(x)$ is inserted into (1), it yields a final expression of the magnetic load $q_{\mathrm{DES}}(x)$. In our case, the breech-fed and the three spatially different DES regimes were examined (see Fig. 3). It was noted that the breech-fed pressure profile [see Fig. 3(a)] represents the envelope, i.e., the maximum values of the DES pressures shown in Fig. 3(b) and (c).

The time-dependent pressure profiles were calculated for the same measured current profiles [8] in all four cases. The second parts of the DES pressure profiles were generated at three time instants of current injections, i.e., $t_1 = 1.18$ ms, $t_2 = 1.92$ ms, and $t_3 = 2.14$ ms which were characterized by the three positions of the second injection point B: $x_{B1} = 32.8$ cm, $x_{B2} = 98.4$ cm, and $x_{B3} = 123.3$ cm (see Fig. 2).

IV. MODELING APPROACH

The computational model's finite element 2D model, which was applied in the further transient finite-element analysis of the rail-gun structure, is presented in Fig. 4.

The rail-gun structure resting on discrete elastic supports was considered as a planar stress bimaterial problem. The T-shaped cross-sectional profile is shown in Fig. 1(b).

The distributed load which was accumulated by the magnetic pressure is attached above the sliding surface of the rail. The values of the distributed load $Q(x,t)$ are recalculated from pressure $q(x,t)$ defined in (1) by accounting the rail size b.

The dynamical behavior of the rail is governed by the linear transient model. By using the matrix notations of the FEM, this

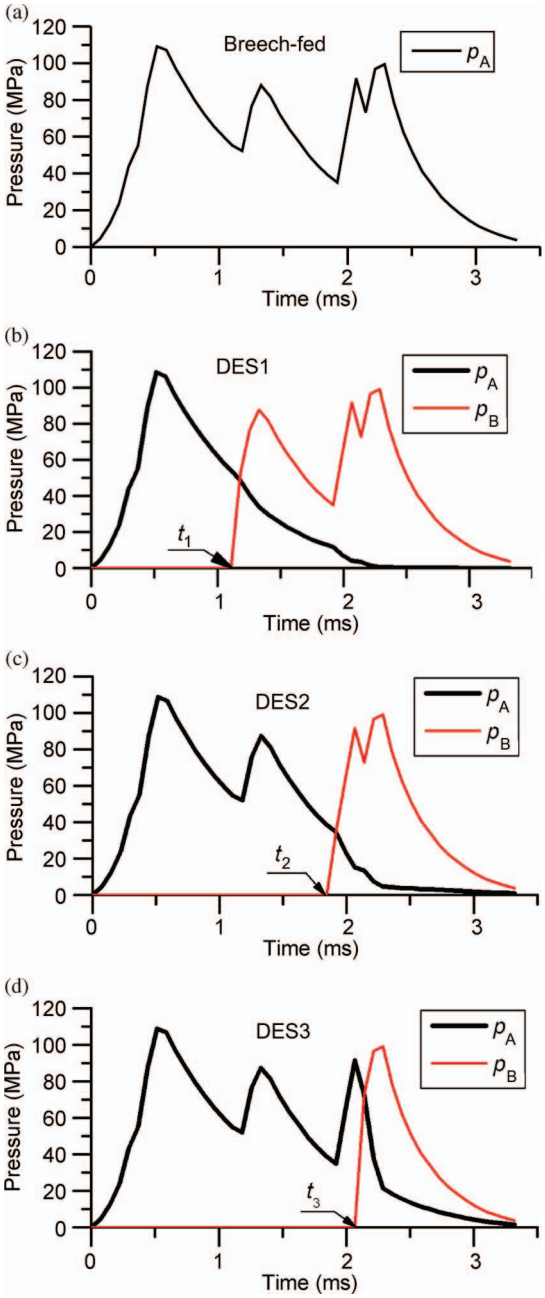

Fig. 3. Time variations of load pressure for (a) breech-fed and for DES modes with various locations of the second injection point B: (b) $x_{B1} = 32.8$ cm, (c) $x_{B2} = 98.4$ cm, and (d) $x_{B3} = 123.3$ cm.

is written as an equation of motion

$$[\boldsymbol{M}]\ddot{\boldsymbol{u}} + [\boldsymbol{K}]\boldsymbol{u} = \boldsymbol{F}_N(t). \tag{4}$$

Here, $\boldsymbol{u}$ represents the unknown nodal values of the time-dependent displacement vector, $\ddot{\boldsymbol{u}}$ is the acceleration, $[\boldsymbol{K}]$ is the linear stiffness matrix, $[\boldsymbol{M}]$ is the mass matrix, and $\boldsymbol{F}_N(t)$ is the vector of the external time-dependent electromagnetic load. The damping term was not considered in this equation; thus, overestimated dynamic effects were obtained. The numerical analysis of this mechanical model was conducted using the FEM software ANSYS [12]. The finite-element mesh that was used consisted of 18 652 2D plane quadrilateral elements. The whole model had 56 719 degrees of freedom.

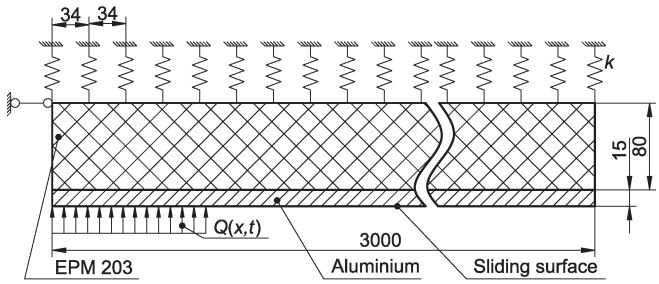

Fig. 4. Two-dimensional model of the rail gun on discrete supports.

V. Numerical Results

This section presents the results of the numerical analysis of the ISL rail-gun EMA3 under the four previously described loading profiles. The solution of the governing dynamic equation (4) yields the time variations of the displacements in all nodes of the FEM model.

The aim of the structural analysis that was performed was to study an important aspect of the rail–armature contact interface, namely the deflections of the inner rail surfaces due to the magnetic pressure mentioned earlier.

It should be noted that even small changes of the deflection magnitude in a range of some tenths of millimeters can be significant. In the case of compression, this can be attributed to the effects of friction and gauging at the sliding contact. In the case of detachment, it can be the characteristic of the efficiency of the load transmission.

The first case study concerned the analysis of the rail gun under breech-fed loading. The most representative results of this transient analysis are presented as a 2D plot in the time and length plane t–x. The variations of the contact displacement or deflections of the inner rail surfaces are presented in Fig. 5(a).

Further studies concerned the analysis of the rail gun under the three loading regimes DES1, DES2, and DES3. The 2D plots of the time variation of the displacement of the rail surface are presented in Fig. 3(b)–(d), respectively. All three graphs are identical to the previous sample. Here, the gray-color scale indicates the displacement magnitude. The solid line indicates the path of the projectile shown in Fig. 2. The tangent of the curve indicates the instantaneous velocity $v = \tan\alpha$.

These pictures show the characteristic behavior of the rail gun under these four peak loading profiles. The curve of the projectile path divides plane t–x into two areas. The almost homogeneous dark area above the curve corresponds to the practically nondeformed surface behavior ahead of the projectile while the area below the curve corresponds to the deformed surface behavior behind the projectile. It should be mentioned that line $t = t_{\rm cr}$ separates precritical $(t < t_{\rm cr})$ and postcritical $(t > t_{\rm cr})$ motions.

During the precritical motion, the speed of the waves is apparently higher than that of the projectile. The reflection and interference of these waves in the end of the rail zone were observed.

In the postcritical phase, the character of the woven pattern of the displacement field observed in the picture ahead of the projectile indicates the propagation of waves with a constant critical velocity.

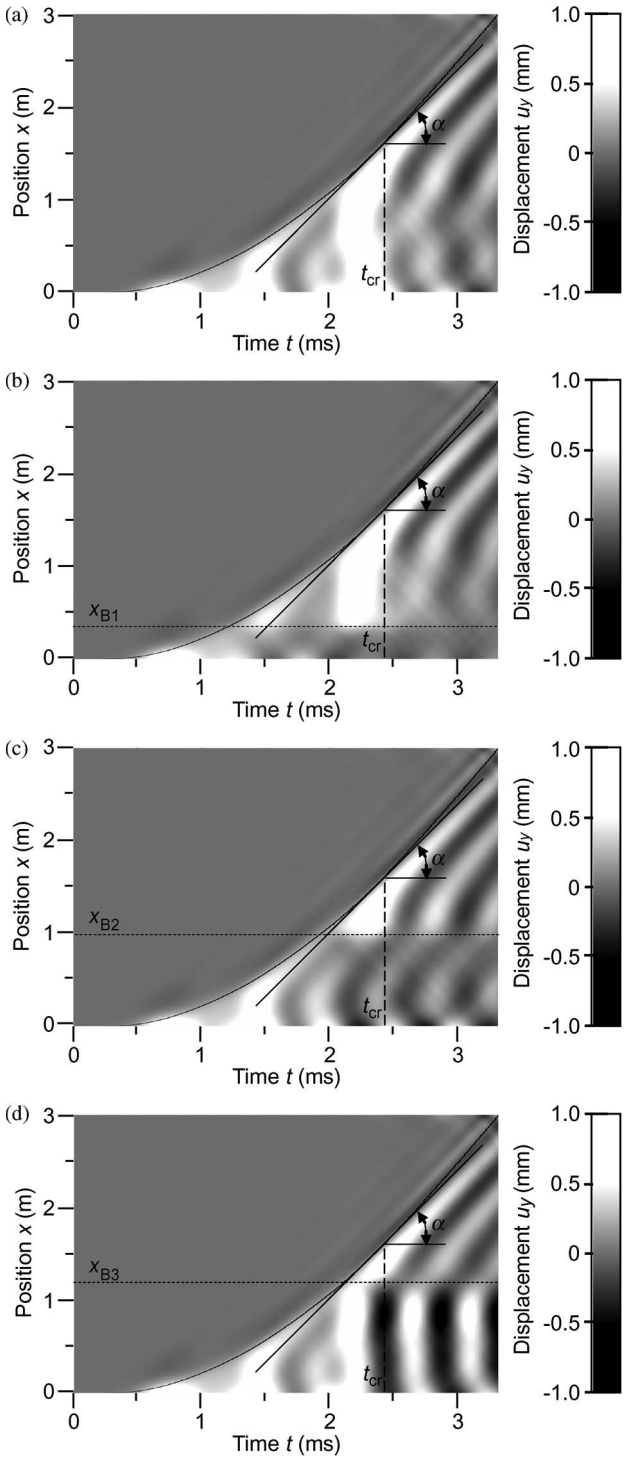

Fig. 5. Two-dimensional time–length variation of rail surface displacements under various loads. (a) Breech-fed. (b) DES1. (c) DES2. (d) DES3.

Generally, these pictures exhibit similar tendencies concerning the propagation and interference of the waves ahead of the projectile; however, visible differences were detected below the critical velocity. These indicate the influence of the injection point positions denoted by x_{B}.

VI. Analysis and Discussion

The 2D plot of the displacement profile shown in Fig. 5 is suitable only for a qualitative examination but cannot be used for analysis purposes. For the detailed characterization of the rail-gun surface, the envelope profiles of the displacement under the four load regimes were plotted. These are shown in Fig. 6.

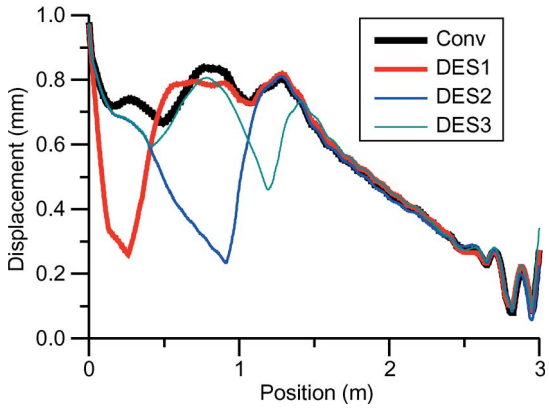

Fig. 6. Envelope of displacements of the sliding surface along the rail for various load regimes.

Each point of the graphs presents the maximal values of the displacement obtained at position x during the entire loading history. These graphs confirm that these displacements are not very sensitive to the various loadings in front of the projectile. The oscillations at the final stage may be interpreted as the result of the wave reflection and the interference of the waves in the end of the rail.

Considerable differences were observed, however, behind the projectile. The conventional breech-fed mode had the highest displacement values. The DES loads yielded lower values. These are desirable in a device having a longer life perspective.

To enhance the characterization of these problem-oriented parameters, the use of the averaged quasi-contact displacement $\overline{u}_N$ is suggested. $\overline{u}_N(t)$ characterizes the surface deflections related to the positions of the projectile in time t and represents the average values of the projectile–rail contact displacement $\overline{u}_N(x)$.

This parameter is obtained as the integrated parameter of the loaded surface

$$\overline{u}_N\left(x_f(t)\right) = \frac{1}{L_{\mathrm{proj}}} \int\limits_{x_f - L_{\mathrm{proj}}}^{x_f} u_N(x)dx. \tag{5}$$

Here, $L_{\mathrm{proj}} = 5$ cm is the projectile length while $x_f(t)$ is the location of the loading front defined by (2).

The time variations of the average contact displacement obtained under action of all the four loadings are presented in Fig. 7(a). The obtained displacement profiles are characterized by three peaks. The first displacement peak with the highest value equal to 0.6 mm is caused by the first load peak while the third peak is caused by the interaction of the third and fourth load peaks. The final stage is characterized by negative values, which means that the rails approach each other.

This averaging approach was also used to characterize the rail deformation behavior ahead of the projectile. The averaged parameter similar to that of (5) was suggested. It reflects the displacement field of up to $L_{\mathrm{proj}} = 6$ cm in front of the projectile. The time variations of the average contact displacement obtained under action of all four loadings are presented in Fig. 7(b).

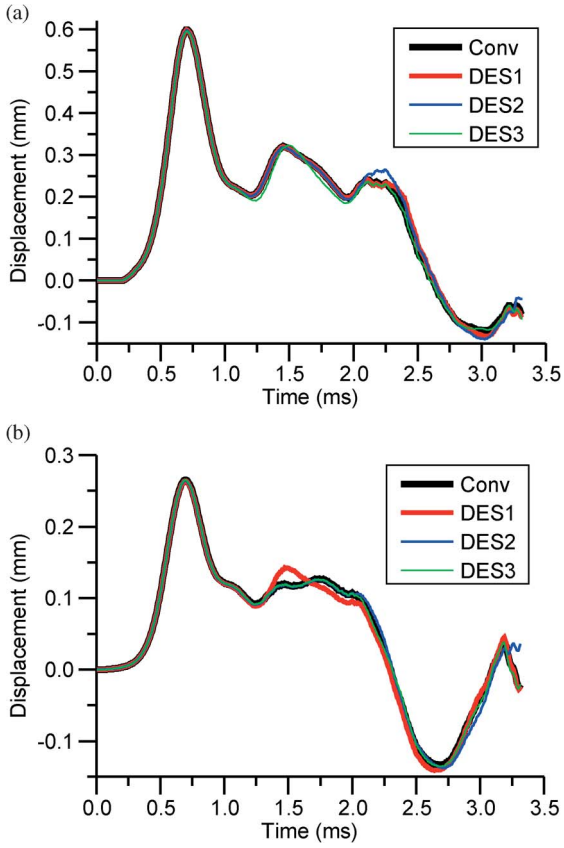

Fig. 7. Variations of the average contact displacements amplitude in time for different load regimes. (a) Under projectile. (b) In front of the projectile.

VII. Concluding Remarks

The structural mechanics of the existing rail gun with discrete supports were analyzed using a 2D FE model. Experimentally obtained pressure curves were used to simulate the breech-fed loading and three different DES loadings.

The presented results have illustrated qualitatively and quantitatively the deformation behavior of the rails. The characterization of the sliding surface deflections in terms of displacements has revealed extreme values near the muzzle.

This paper did not find significant differences between the breech-fed and DES loadings under the projectile. Since DES is known to improve the launch efficiency and is not disadvantageous with respect to the structural mechanics of the rail-gun system as a whole, it is the preferable operation mode for the configurations considered in this paper.

References

[1] L. Tumonis, M. Schneider, R. Kacianauskas, and A. Kačeniauskas, "Structural mechanics of railguns in the case of discrete supports," *IEEE Trans. Magn.*, vol. 45, no. 1, pp. 474–479, Jan. 2009.

[2] A. J. Johnson and F. C. Moon, "Elastic waves and solid armature contact pressure in electromagnetic launchers," *IEEE Trans. Magn.*, vol. 42, no. 3, pp. 422–429, Mar. 2006.

[3] A. J. Johnson and F. C. Moon, "Elastic waves in electromagnetic launchers," *IEEE Trans. Magn.*, vol. 43, no. 1, pp. 141–144, Jan. 2007.

[4] J. T. Tzeng and W. Sun, "Dynamic response of cantilevered rail guns attributed to projectile/gun interaction—Theory," *IEEE Trans. Magn.*, vol. 43, no. 1, pp. 207–213, Jan. 2007.

[5] L. Tumonis, R. Kacianauskas, A. Kačeniauskas, and M. Schneider, "The transient behaviour of rails used in electromagnetic rail guns: Numerical investigations at constant loading velocities," *J. Vibroeng.*, vol. 9, no. 3, pp. 15–19, Jul.–Sep. 2007.

[6] K.-T. Hsieh, S. Satapathy, and M.-T. Hsieh, "Effects of pressure-dependent contact resistivity on contact interfacial conditions," *IEEE Trans. Magn.*, vol. 45, no. 1, pp. 313–318, Jan. 2009.

[7] R. Marshall and W. Ying, *Railguns: Their Science and Technology*. Beijing, China: China Machine Press, 2004.

[8] M. Schneider and R. Schneider, "Sliding contact performance of multiple brush armatures," *IEEE Trans. Magn.*, vol. 41, no. 1, pp. 432–436, Jan. 2005.

[9] M. Schneider, D. Eckenfels, and F. Hatterer, "Transition in brush armatures," *IEEE Trans. Magn.*, vol. 39, no. 1, pp. 76–81, Jan. 2003.

[10] L. Tumonis, M. Schneider, R. Kacianauskas, and A. Kačeniauskas, "Comparison of dynamic behaviour of EMA-3 railgun under differently induced loadings," *Mechanika*, vol. 78, no. 4, pp. 31–37, 2009.

[11] M. Schneider and R. Schneider, "Rail-sabot configurations for brush armatures," *IEEE Trans. Magn.*, vol. 43, no. 1, pp. 186–189, Jan. 2007.

[12] *ANSYS. Reference Manual*, 8th ed. Canonsburg, PA: SAS IP INC., 2003.

Liudas Tumonis received the Ph.D. degree in mechanical engineering from the Vilnius Gediminas Technical University, Vilnius, Lithuania. in 2010.

Since 2010, he has been a Research Fellow with the Vilnius Gediminas Technical University. He has coauthored four scientific papers. His research interests include finite-element method, discrete-element method, and applications in structural and mechanical engineering.

Markus Schneider received the Ph.D. degree in physics from the University of Jena, Jena, Germany, in 1998.

Since 1999, he has been with the French–German Research Institute of Saint Louis (ISL), Saint Louis, France, where he was a Project Manager in a multidisciplinary effort on plasma physics in conventional combustion-driven accelerators and electromagnetic rail guns from 2004 to 2009. Since 2007, he has been the Head of the Electromagnetic Acceleration Group with ISL. He has authored and coauthored more than 50 scientific papers. He is the holder of three patents. His research interests include pulsed power, sliding electric contacts, innovative metrology, and terahertz physics.

Rimantas Kačianauskas received the Ph.D. degree in structural engineering from the Vilnius Gediminas Technical University, Vilnius, Lithuania, in 1982.

Since 1975, he has been with the Vilnius Gediminas Technical University, where he started his scientific activities. Since 1995, he has been a Professor and the Head of the Department of Strength of Materials with the Vilnius Gediminas Technical University. He is the author and coauthor of more than 150 scientific publications. His research interests include finite-element method, discrete-element method, structural dynamic, mechanics of materials, fracture mechanics, and coupled problems.

Vaidas Vadluga received the Ph.D. degree in mechanical engineering from the Vilnius Gediminas Technical University, Vilnius, Lithuania, in 2008.

Since 2008, he has been a Research Fellow with the Vilnius Gediminas Technical University. He has coauthored five scientific papers. His research interests include dynamic processes, finite-element method, discrete-element method, and fracture mechanics.